A new angle-domain imaging condition for prestack reverse-time migration

Rui Yan and Xiao-Bi Xie, IGPP, University of California, Santa Cruz, CA 95064*

Summary

Based on the full-wave equation, reverse time migration (RTM) can handle wave propagation in all directions without angle limitation. However, the wide-angle capability of full-wave propagator creates artifacts in migrated image if the conventional imaging condition (zero-lag cross-correlation) is applied. In this paper, we propose a new imaging condition to attenuate these artifacts by decomposing the full wavefields at every image location to local plane waves of different directions, followed by constructing the image by correlating certain combinations of the plane-wave components. Synthetic examples demonstrate that this imaging condition can effectively remove the undesired artifacts in both simple and complex model.

Introduction

Reverse time migration (RTM) has spurred much interest in recent years because of the increased imaging challenges posed by complex subsurface targets and affordable computer resources such as Linux clusters.

As a wave equation technique using full-wave equation, the RTM can handle not only multi-arrivals but have no dip limitation, enabling imaging of overturned reflections. However, the RTM is known for producing low-wavenumber artifacts, which often mask the geological structures. Those artifacts result from the unwanted cross-correlation of head waves, diving waves and backscattered waves at the imaging step (Yoon et al., 2004). These events are particularly serious where high velocity contrasts or high velocity gradient exist.

Several approaches have been proposed to suppress the image artifacts resulted from conventional imaging condition. In post-stack RTM, these artifacts can be effectively suppressed by matching the impedance of the media, i.e., utilizing the non-reflecting wave equation (Baysal et. al, 1984) or by smoothing the velocity model to reduce the reflections (Loewenthal, et. al, 1987). However, both approaches become less effectively under the prestack scenario, because it is hard to simultaneously match non-reflection conditions for broad incident angles. Guitton et al. (2006) used different post-imaging filters to remove the image artifacts, e.g., Laplacian filter, derivative filter and least square filter. Fletcher et al. (2005) attenuated reflections at boundaries by introducing a directional damping term to the non-reflecting wave equation during propagation.

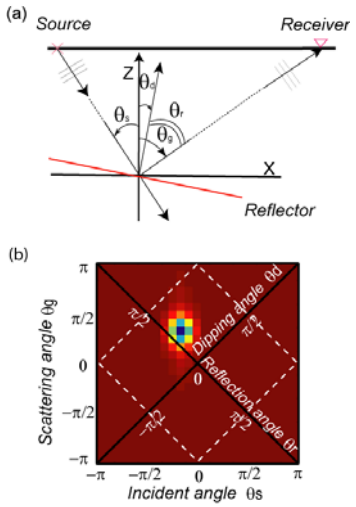

Figure 1: Sketch showing the calculation of local image matrix (a) Coordinate system used in local angle-domain analysis (b) a local image matrix. The horizontal and vertical coordinates are incidence and scattering angles while the two diagonals are dipping angle and reflection angle, respectively.

Angle related image conditions have been tested by several authors to be a more effective method to suppress the image artifacts. Under this category, Yoon et al. (2004) used an angle-related weighting function to sort the source and receiver waves based on their incoming direction. The angle information is calculated from Poynting vectors of source and receiver waves. Only the energy actually related to the reflections is kept in the imaging. Xie and Wu (2006) proposed a full-wave coupled with one-way method to solve the image problem, where the wavefield generated by the full-wave method is decomposed into one-way components at different directions. Then the image condition is applied to the proper combinations of the wave components for imaging. Liu et al. (2007) also explored the angle-domain image condition. Denli and Huang (2008) extended the method to the elastic wave case.

In the above mentioned angle-domain image conditions, the wave propagation direction is extracted using the differentiation method. In a complex model, different wavefields often coexist and overlap with each other. The differentiation method sometimes fails to give the right directional information for the propagating wavefield. In this paper, we propose a new angle-domain imaging condition for prestack RTM, in which the angle

information is extracted using a slant stack method. Besides, we construct the local imaging matrix (LIM) which provides a clear picture to separate the images from the migration artifacts.

Methodology

The conventional imaging condition is designed to extract the location of subsurface reflectors where propagation times from source and receivers match. It can be easily expressed as

$$I(\mathbf{x}) = \int_0^T S(\mathbf{x},t)R(\mathbf{x},T-t)dt, \quad (1)$$

where T is the total recording time, $S(\mathbf{x},t)$ and $R(\mathbf{x},T-t)$ are source wavefield and receiver wavefield, respectively.

In a complex velocity model, the reflection, scattering, multi-pathing, etc., make the source and receiver waves come to a given location from various directions. The conventional image condition composes of energy from all directions without separating it. To build an angle-domain imaging condition, we have to decompose the source and receiver waves into many local plane waves (or beams) along different directions. Then we choose plane-wave members from source and receiver wavefields to construct the angle domain partial image. We use the local slant stacks technique to decompose the source and receiver wavefields into superposition of local plane waves. It can be formulated as below (Xie et al., 2005; Yang and Xie, 2008):

$$G(\theta,\mathbf{x},\tau) = \frac{C(\tau,\theta)}{N}\sum_{i=1}^{N} W(\mathbf{x}_i' - \mathbf{x})G\left[\mathbf{x}_i', t = \tau + \mathbf{p}\bullet(\mathbf{x}_i' - \mathbf{x})\right], \quad (2)$$

where $G(\mathbf{x},\tau)$ stands for either source wavefield $S(\mathbf{x},\tau)$ or receiver wavefield $R(\mathbf{x},\tau)$. $G(\theta,\mathbf{x},\tau)$ is its decomposed local plane wave whose propagating direction is θ, W is a spatial window function centered at point $\mathbf{x}$. N is the number of traces used in this calculation. $\mathbf{p} = (\sin\theta/v, \cos\theta/v)$ is slowness vector, v is average velocity within the spatial window. $C(\tau,\theta)$ was introduced by Bradshaw and Ng (1987) to improve the resolution of slant stacks . It is defined as

$$C(\tau,\theta) = \frac{\sum_l (\sum_{i=1}^{N} u_i(\tau,\theta))^2}{N \cdot \sum_l \sum_{i=1}^{N} u_i^2(\tau,\theta)}, \quad (3)$$

where $u_i(\tau,\theta) = W(\mathbf{x}_i' - \mathbf{x})G[\mathbf{x}_i', t = \tau + \mathbf{p}\bullet(\mathbf{x}_i' - \mathbf{x})]$, l is a window size and is usually a wavelet length. $C(\tau,\theta)$ is independent of the amplitude of N traces and ranges from 0 to 1. It can enhance the strength of coherent signals and weaken that of incoherent ones. As an important factor, it can help to prevent the smearing effect of slant stacks.

By applying the image condition to the decomposed local plane waves, we obtain the partial image in angle-domain

$$I(\theta_s,\theta_g,\mathbf{x}) = \int_0^T S(\theta_s,\mathbf{x},t)R(\theta_g,\mathbf{x},T-t)dt. \quad (4)$$

The partial image at location $\mathbf{x}$ is relate to an incident plane wave along θ_s and a scattering plane wave along θ_g. Collecting all possible pairs of θ_s and θ_g, the partial images form a matrix $I(\theta_s,\theta_g,\mathbf{x})$ called local imaging matrix (LIM). The acquisition coordinate (θ_s,θ_g) can be converted into the target coordinate (θ_r,θ_d) through transform $\theta_d = (\theta_s + \theta_g)/2$ and $\theta_r = (\theta_s - \theta_g)/2$, where θ_d is the local dipping angle and θ_r is the local reflection angle. The sketch in Figure 1a shows the relationship between these angles. Illustrated in Figure 1b is the structure of a 2D LIM, where the horizontal and vertical coordinates are incident and scattering angles, the main diagonal is the reflection angle, and the secondary diagonal is the dip angle. Note that for a one-way propagator, the maximum incident, scattering, dip and reflection angles in the LIM can only reach to $\pm\pi/2$. In contrast, in RTM, the full-wave propagator can make the incident, scattering, dip and reflection angles in the LIM all the way to $\pm\pi$.

The low-wavenumber artifacts in RTM are usually generated by correlations between diving waves and their time reversed counterparts along wave paths. These events appear as very wide angle "reflections" with their reflection angles are nearly $\pi/2$. In LIM, it is easy to understand why the RTM causes serious artifacts but a one-way migration does not. That is simply because a one-way propagator does not extend to wide angle range which includes the near $\pi/2$ reflections. In RTM, people usually sum up all the elements, i.e., the partial images, in the LIM to construct the image $I(\mathbf{x})$, i.e.,

$$I(\mathbf{x}) = \sum_{\theta_r}\sum_{\theta_d} I(\theta_r,\theta_d,\mathbf{x}). \quad (5)$$

However, in this way, the wide-angle events will enter the image and cause artifacts. Instead, we can filter the very wide-angle energy to eliminate the low-wavenumber artifacts in the image. Based on this consideration, our angle-domain imaging condition can be expressed as

$$I(\mathbf{x}) = \sum_{\theta_r}\sum_{\theta_d} M(\theta_r,\theta_d) I(\theta_r,\theta_d,\mathbf{x}), \quad (6)$$

where $M(\theta_r,\theta_d)$ is an angle domain filter which blocks the very wide-angle events from entering the image. For example, we can choose to block all events with local reflection angles larger than $\pi/4$ from entering the LIM. It

A new angle-domain imaging condition for reverse-time migration

is possible that we design more flexible angle-domain filters. For example, filters can be target oriented or depth dependent. We can even adjust filters for different image points according to the behavior of artifacts in preliminary images.

Numerical Examples

Shown in Figure 2 is a simple velocity model used to demonstrate the application of the new imaging condition. The model is composed of a background with a vertical velocity gradient and a salt dome with steep flanks. The acquisition system contains 21 shots with double-side receivers and the maximum number of receivers for one shot is 300. A 2D fourth-order full-wave finite-difference code is used to generate the synthetic data. The data are preprocessed by muting the direct arrivals and tapering the data in space to reduce aperture-edge effects.

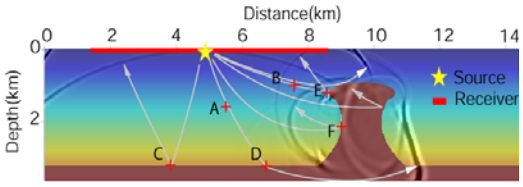

Figure 2. Velocity model used to demonstrate the new image condition. Overlapped in the figure is the snapshot from a single shot. The rays explain different waves generated in the model.

We first investigate the characteristics of energy distributions for the true images and artifacts in the local imaging matrices. Illustrated in the center of Figure 3 is the RTM image for the salt dome model generated from a single shot using the conventional image condition. The major phases and ray paths from this shot can also be seen from the overlapped snapshot and ray paths in Figure 2. As expected, the RTM image properly imaged the horizontal interface. The nearly vertical salt flank and part of the salt cap are properly imaged because the RTM method can correctly calculate the turning waves in a model with velocity gradient. However, the turning wave in the model also generates strong artifacts which contaminate the image. To illustrate the characteristics of energy distributions, the LIMs at selected location in the model are calculated and presented in Figure 3. These LIMs are labeled from A to F with their locations indicated in the model.

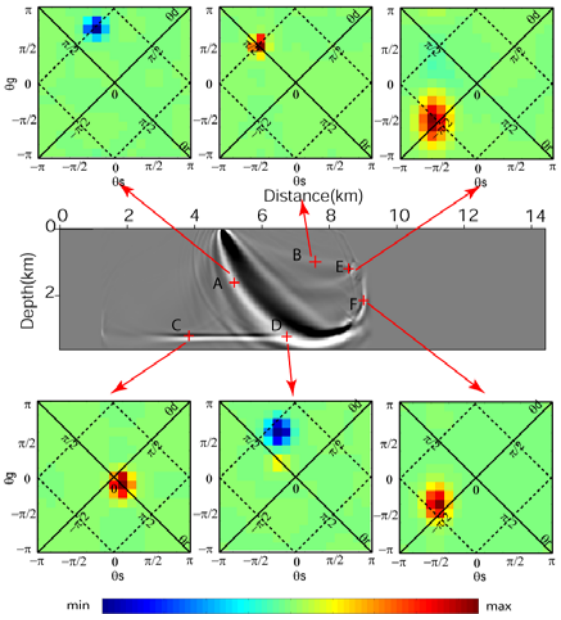

Figure 3. The RTM image for the salt dome model generated using a single shot and conventional image condition. The image matrices for selected locations in the figure are calculated. The energy for the image and artifacts show different behavior in LIM.

The points A and B do not relate to any real targets but dominated by strong artifacts generated from turning waves. The LIMs calculated for these locations show that the energy is concentrated at reflection angle $\theta_r = \pi/2$. These artifacts are generated by incident turning wave and back-propagated turning waves from both source and receiver sides. They reach to the image point nearly parallel but with opposite directions. In a long range, these signals will correlated and generate strong image artifacts. The energy distributed at reflection angle $\pm\pi/2$ correctly describes their property. The point C is located on the horizontal interface and the energy distribution reveals it is properly imaged by near vertical incident and scattered waves. The dipping angle is zero (refer to Figure 1). At points E and F, the energy distribution show that the target dipping angle is nearly $-\pi/2$ and the image is generated by near normal incident waves, i.e., their reflection angles are nearly zero. Point D is located on the target. There are two clusters of energy in its image matrix. One is generated by reflection energy which located at zero dipping angle and near 40 degree reflection angle. The other is generated by artifacts which has a near $\pi/2$ reflection angle.

A new angle-domain imaging condition for reverse-time migration

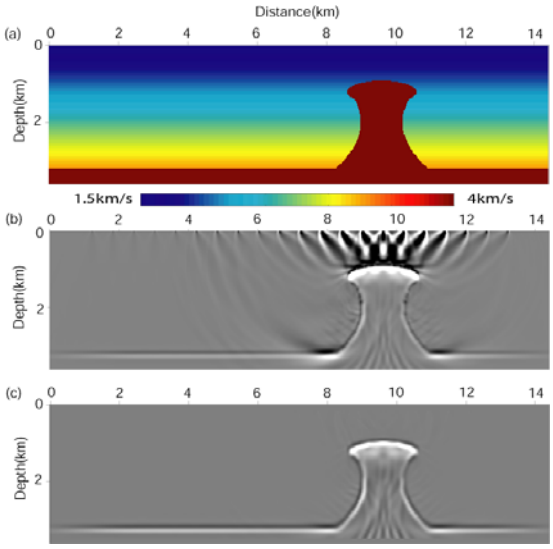

Figure 4. Comparison between the prestack depth image using different image conditions, with a) the velocity model, b) the multi-shot image using the conventional image condition, and c) the image using new imaging condition. Note the migration artifacts are mostly removed.

These results show that the energy distribution in LIM is closely related to the local angle information of seismic events. The reflection signal and artifacts show different behavior in the LIM. If we apply the imaging condition (6) in image matrixes, artifacts can be attenuated while reflection information can be preserved. Illustrated in Figure 4 are velocity model and prestack depth images. Figure 4b is the prestack depth image calculated using the conventional image condition. Both the horizontal interface and the vertical flank of the salt dome are clearly imaged. However, there are strong long wavelength artifacts on the top and both sides of the salt body. These artifacts prevent us from obtaining detailed structures in these areas. In Figure 4c, the new image condition proposed in this paper has been applied and the result shows improved image. Most of those long wavelength migration artifacts disappear, while the image of reflector is well preserved.

Next, we test this image condition on the 2D BP dataset (Billette et al. 2005). Figure 5a shows the image for part of the model. Although the boundary of the salt body can be seen in the figure, the region above the salt is strongly contaminated by the migration artifacts. The shallow structures are nearly invisible due to large-amplitude artifacts. Figure 5b is the result obtained by using the new imaging condition. The shallow part, especially the sediment structures, becomes identifiable.

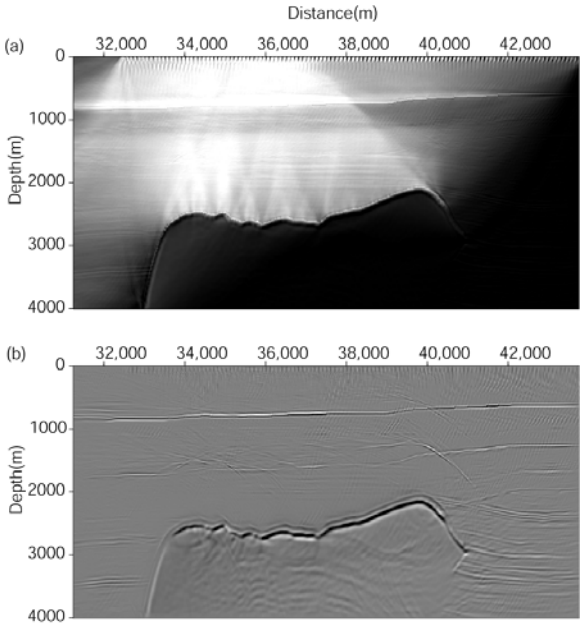

Figure 5: Prestack depth image for part of the BP data set, with a) the image using the conventional imaging condition, and (b) using the new angle-domain image condition.

Conclusion and Discussion

In this paper, an angle-domain imaging condition is proposed for prestack RTM. We decompose the full wavefields into local plane wave components using local slant stacks technique and apply an imaging condition by taking account of local angle information. Numerical examples show that the artifacts caused by conventional imaging condition are significantly removed. The imaging procedure described in this paper is implemented in time domain, requiring great computing cost and disk storage. Furthermore, several parameters, for example, the number of angles, the size of local window and wavefield sampling in space and time to apply local slant stacks, must be chosen appropriately to compromise between the image quality and computation efficiency.

Acknowledgements

This research is supported by the WTOPI Consortium at the University of California, Santa Cruz. The facility support from the W.M. Keck Foundation is also acknowledged.

EDITED REFERENCES

Note: This reference list is a copy-edited version of the reference list submitted by the author. Reference lists for the 2009 SEG Technical Program Expanded Abstracts have been copy edited so that references provided with the online metadata for each paper will achieve a high degree of linking to cited sources that appear on the Web.

REFERENCES

Baysal, E., D. D. Kosloff, and J. W. C. Sherwood, 1983, Reverse time migration: Geophysics, **48**, 1514–1524.

———, 1984, A two-way nonreflecting wave equation: Geophysics, **49**, 132–141.

Billette, F., and S. Brandsberg-Dahl, 2005, The 2004 BP velocity benchmark: 67th Annual Conference and Exhibition, EAGE, Extended Abstracts, B035.

Bradshaw, A., and M. Ng, 1987, Multiple attenuation by parabolic stack Radon transform: Geo-X System Internal Paper.

Denli H., and L. Huang, 2008, Elastic-wave reverse-time migration with a wavefield-seperation imaging condition: 78th Annual International Meeting, SEG, Expanded Abstracts, 2346–2350.

Fletcher, R. P., P. J. Fowler, and P. Kitchenside, 2005, Suppressing artifacts in prestack reverse time migration: 75th Annual International Meeting, SEG, Expanded Abstracts, 2049–2051.

Guitton, A., B. Kaelin, and B. Biondi, 2006, Least-square attenuation of reverse-time migration artifacts: 76th Annual International Meeting, SEG, Expanded Abstracts, 2348–2352.

Liu, F., G. Zhang, S. A. Morton, and J. P. Leveille, 2007, Reverse-time migration using one-way wavefield imaging condition: 77th Annual International Meeting, SEG, Expanded Abstracts, 2170–2174.

Loewenthal, D., P. A. Stoffa, and E. L. Faria, 1987, Suppressing the unwanted reflections of the full wave equation: Geophysics, **52**, 1007–1012.

Xie, X. B., Z. Ge, and T. Lay, 2005, Investigating explosion source energy partitioning and Lg-wave excitation using a finite-difference plus slowness analysis method: Bulletin of the Seismological Society of America, **95**, 2412–2427.

Xie, X. B., and R. S. Wu, 2006, A depth migration method based on the full-wave reverse-time calculation and local one-way propagation: 76th Annual International Meeting, SEG, Expanded Abstracts, 2333–2337.

Yang, H., and X. B. Xie, 2008, Target oriented full-wave equation based illumination analysis: 78th Annual International Meeting, SEG, Expanded Abstracts, 2216–2220.

Yoon, K., K. Marfurt, and E. W. Starr, 2004, Challenges in reverse-time migration: 74th Annual International Meeting, SEG, Expanded Abstracts, 1057–1060.